Engineering of a Microscale Niche for Pancreatic Tumor Cells Using Bioactive Film Coatings Combined with 3D-Architectured Scaffolds

Arunkumar Rengaraj, Lauriane Bosc, Paul Machillot, Colin Mcguckin, Clément Milet, Nico Forraz, Philippe Paliard, Denis Barbier, Catherine Picart

ENGINEERING OF A MICROSCALE NICHE FOR PANCREATIC TUMOR CELLS USING BIOACTIVE FILM COATINGS COMBINED WITH 3D-ARCHITECTURED SCAFFOLDS

*Arunkumar Rengaraj[ab#], Lauriane Bosc[ab#], Paul Machillot[ab], Colin McGuckin[c], Clément Milet[c], Nico Forraz[c], Philippe Paliard[d], Denis Barbier[d] and Catherine Picart [abe]**

[a] *Univ. Grenoble Alpes, INSERM U1292, CEA, CNRS EMR 5000 BRM, IRIG Institute, CEA, Bât C3, 17 rue des Martyrs, 38054, Grenoble, France.*

[b] *Grenoble Institute of Engineering, CNRS UMR 5628, LMGP, 3 parvis Louis Néel, 38016 Grenoble, France*

[c] *Cell Therapy Research Institute, CTIBiotech, 5 avenue Lionel Terray, 69330 Meyzieu, France*

[d] *Microlight 3D, 5 avenue du Grand Sablon, 38700 La Tronche, France*

[e] *Institut Universitaire de France (IUF), Ministère de l'Enseignement Supérieur, de la Recherche et de l'Industrie, 1 rue Descartes, 75 231 Paris Cedex 05, France*

[#] these authors contributed equally to this work.

***Corresponding author:** Catherine PICART catherine.picart@cea.fr, INSERM U1292 Biosanté, CNRS EMR 5000 BRM, IRIG Institute, CEA bât C3, 17 rue des Martyrs, F-38054 Grenoble.

Keywords: Tissue engineering, biomimetism, niche, pancreatic cancer, growth factors, surface coating, cell adhesion, and proliferation.

Abstract

Two-photon polymerization has recently emerged as a promising technique to fabricate scaffolds for 3D cell culture and tissue engineering. Here, we combined a 3D-printed microscale scaffolds fabricated using two-photon polymerization with a bioactive layer-by-layer film coating. This bioactive coating consists of hyaluronic acid and poly(L-lysine) of controlled stiffness, loaded with fibronectin and bone morphogenic proteins 2 and 4 (BMP2 and BMP4) as matrix-bound proteins. Planar films were prepared using a liquid handling robot directly in 96-well plates to perform high-content studies of cellular processes, especially cell adhesion, proliferation and BMP-induced signaling. The behavior of two human pancreatic cell lines PANC1 (immortalized) and PAN092 (patient-derived cell line) were systematically compared and revealed important context-specific cell responses, notably in response to film stiffness and matrix-bound BMPs (bBMPs). Fibronectin significantly increased cell adhesion, spreading, and proliferation for both cell types on soft and stiff films, BMP2 increased cell adhesion and inhibited proliferation of PANC1 cells and PAN092 on soft films. BMP4 enhanced cell adhesion and proliferation of PANC1 and showed a bipolar effect on PAN092. Importantly, PANC1 exhibited a strong dose-dependent BMP response, notably for bBMP2, while PAN092 were insensitive to BMPs. Finally, we proved that it is possible to combine a microscale 3D Ormocomp scaffold

fabricated using the two-photon polymerization technique with the bioactive film coating to form a microscale tumor tissue and mimic the early stages of metastatic cancer.

Introduction

Pancreatic cancer is the seventh leading cause of cancer-related death in humans, with a 91% mortality rate within five years of diagnosis. In 2018, nearly 432,000 new deaths related to pancreatic cancer were reported worldwide[1]. This high mortality rate is due to the lack of diagnostic tools and limitations of existing models used to study cancer cell mechanisms. Classical culture plates (TCPS) are unable to mimic the biophysical and chemical conditions of the tumor microenvironment[2]. Moreover, these models are not physiological because the cells are cultured on stiff materials such as TCPS or glass. In vivo, the mature tumor is organized in a three-dimensional (3D) architecture and surrounded by an extracellular matrix (ECM). In vivo models have been developed, such as patient-derived xenograft (PDX) mice[3] and genetically modified mice[4]. However, these procedures are lengthy, expensive, and raise many ethical issues related to animal handling. Therefore, there is a need to develop new in vitro platforms that mimic the in vivo tumor microenvironment at all stages of development so that cells can eventually form a three-dimensional (3D) tumor and allow better control and tuning of experimental conditions[5].

Researchers developed various types of 3D tumor models such as spheroids[6], 3D-printed tumor models[7], scaffold-based models[8,9], and microfluidic platforms for preclinical cancer studies[10]. In these methods, it is challenging to obtain a tumor model with uniform size and morphology. For example, in spheroid models, cancer cells are forced to aggregate in a defined space to achieve uniform size and shape[11]. This spatial restriction disrupts the processes of cell adhesion, spreading, and proliferation. In addition, growth factors must be administered in soluble form, which is different from in vivo delivery through the ECM or cell-to-cell. In direct printing of a tumor, the cancer cells are mixed with a bio-ink consisting of polymers and cross-linking agents and 3D printed directly. The cells are thus encapsulated in a polymer matrix to facilitate interactions between them. To solve these problems, it is important to develop a platform that allows the cells to self-organize and proliferate to create the 3D tumor model.

In addition, cancer cells require a suitable environment consisting mainly of ECM proteins for biochemical and structural support, growth factors for cell communication, and stromal cells[12]. The ECM enables cancer cells to communicate with each other through specific biochemical and mechanical signals. Its composition and stiffness have a significant impact on tumor mechanisms[13,14]. These

mechanical and chemical signals from the ECM are converted into biochemical signals involved in cell adhesion and spreading[15]. A number of ECM proteins, including fibronectin, interact with cell mechanoreceptors such as integrins, which influence cancer cell processes such as tumor growth, proliferation, migration, and vascularization[16]. Cancer cells can modulate their integrin heterodimer receptors, making them receptive to signals sent through the extracellular matrix, especially its stiffness[16]. Researchers found a large amount of fibronectin on pancreatic ductal adenocarcinomas (PDA), which play an important role in cancer metastasis and chemoresistance[17]. The bone morphogenic protein (BMPs) family is also emerging as an important factor in pancreatic cancer. BMP2 and BMP4, particularly play a role in angiogenesis and are increasingly targeted in cancer therapy. BMPs bind to specific type I and type II BMP receptors. Upon BMP binding, these receptors form heterodimers and initiate the Smad signaling pathway, which begins with the phosphorylation of Smad1/5 to pSMAD1/5. This phosphorylated pSMAD1/5 forms a complex with Smad4 and is then translocated to the nucleus to initiate transcription of specific genes responsible for regulating cellular mechanisms. In pancreatic cancer, Smad4 mutations are common and have also been cited as factors influencing tumorigenesis. Voornveld et al. also suggested that BMPs enhance the invasive behavior of pancreatic cancer due to the loss of Smad4[18]. They also found that TGF-β family proteins induce phosphorylation of Smad1/5[19]. The above literature shows that cell adhesion and cell spreading significantly affect the Smad signaling pathway.

Polyelectrolyte multilayers (PEM) prepared by the layer-by-layer technique are of interest for tissue engineering due to their composition, which can mimic ECM[20,21]. It is possible to tune the film architecture, thickness, chemistry, and mechanical properties[22] and develop protein-inspired nanofilms[23], biosensors, biomimetics[24], and drug delivery systems[25], especially for proteins and growth factors. Based on previous studies by our group, we have selected films of hyaluronic acid (HA) and poly(L-lysine) (PLL) whose stiffness can be adjusted by changing the concentration of the EDC cross-linking agent[26]. These films can serve as reservoirs to deliver growth factors and proteins to cells locally and over a long period of time[27]. In addition, proteins loaded into the films are also protected from aggregation that is commonly observed when they are in solution. This is particularly important as an altered 3D biochemical structure often leads to a loss of protein function.

In this work, our goal was to create a 3D microenvironment in which cancer cells self-organize and proliferate to form an independent 3D microscale tumor tissue that can be further used for high-content analysis and drug screening. We fabricated a 3D scaffold from the synthetic polymer Ormocomp using two-photon photopolymerization (TPP) to support the structure. Furthermore, the scaffold was functionalized with a multilayer bioactive polyelectrolyte film that mimics simple aspects of ECM (stiffness, protein presentation). **(Figure 1)**. The microscaffold allows cells to migrate and organize their 3D cellular network. Based on our previous studies, we prepared films made of 12

(PLL/HA) layer pairs[27], which were then chemically cross-linked to adjust the stiffness to produce films with an elastic modulus of E0 ~200 kPa and ~400 kPa for soft "EDC30" and stiff "EDC70" films, respectively[26,28,29]. The bioactive coating was built up in 24-well plates on the 3D-architectured patterned scaffold[30], proteins were loaded into the films, and cells were seeded **(Figure 1.A)**. In parallel, for studies with high content cancer cell content, we performed initial cell adhesion, spreading, and proliferation on polyelectrolyte films with two different stiffnesses loaded with proteins on films deposited in 96-well plates. This fabrication process was performed using a recently developed automated liquid robot[31] **(Figure 1.B)** and films loaded with increasing concentrations of the proteins. The stiffness was chosen to match the average elasticity of normal tissue (252 ± 134 kPa) that of the pancreatic tumor (349 ± 222 kPa)[32]. To determine the effects of fibronectin (bFN), bone morphogenetic protein 2 (bBMP2), and bone morphogenetic protein 4 (bBMP4), we additionally loaded these proteins onto the slide. Recently, the effect of BMPs on cancer has been widely discussed due to their emerging role in cancer mechanisms[33]. We compared the cellular response of primary patient-derived pancreatic cancer cells with PANC-1 cells, a commonly studied cell line.

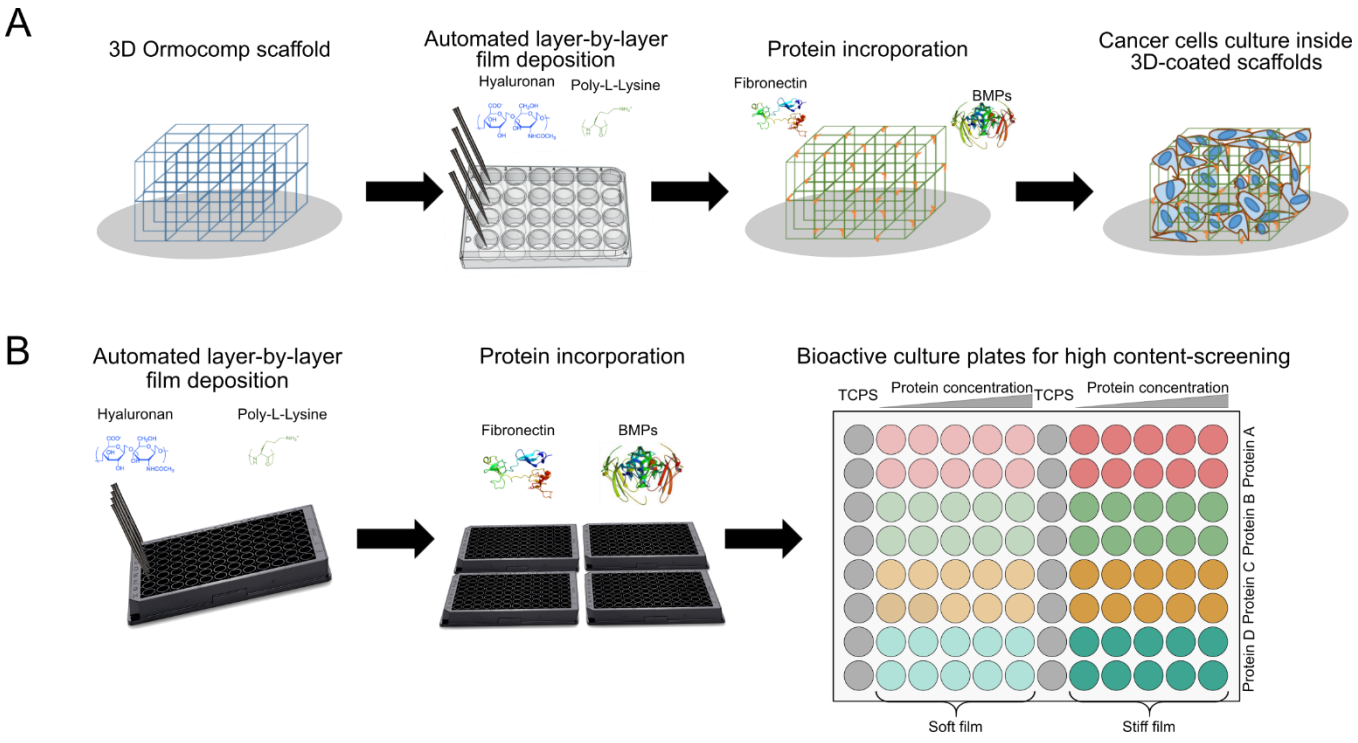

Figure 1. Schematic representation of the overall process of microtumor development on 3D bioactive scaffolds. **(A)** Polyelectrolyte multilayer film coating using a liquid handling robot, protein loading and cell seeding on the 3D Ormocomp scaffold and **(B)** Polyelectrolyte multilayer coating and protein loading on the 96-well plates for high-throughput cellular assays.

MATERIALS & METHODS

Scaffold fabrication using two-photon polymerization technique

The 3D scaffold architecture consists of two floors of 8x8 meshes with a width and height of 120 meters. The design of the scaffold was sliced using Simpoly software (Microlight3D, La Tronche, France). The scaffolds were fabricated with Ormocomp polymer (Micro resist technology, Berlin, Germany) using two-photon polymerization process. The TPP system (µFab3D.Advanced by Microlight3D, La Tronche, France) is equipped with a 20x magnification objective and a numerical aperture of 0.75. A 3D piezoelectric actuator allows the laser focal point set on the Ormocomp resin to initiate polymerization in 3D space. The microchip laser generates femtosecond laser pulses at 532 nm that are highly focused inside the monomer. The TPP is then localized at the focal point in a small volume (~ 1 μm^3) called a voxel. 3D patterning can be achieved by scanning the focal point in a drop of Ormocomp deposited on a Ø14 mm glass coverslip (0.17 mm thick) between two spacers. The laser power was set between 4 and 7.2 mW via software (Lithos, Microlight3D, La Tronche, France). The lateral printing speed was 120 µm/s, and the layer spacing was 300 µm. After polymerization, the residual monomer was removed by washing the sample several times with 90% acetone, leaving the scaffolds on the glass. The scaffolds were designed to maximize cell-cell interaction and molecular diffusion with a minimal hypoxic core.

Polyelectrolyte multilayer film preparation and cross-linking

HA (sodium hyaluronate, MW 360,000 g/mol) was purchased from Lifecore (Chaska, MN, USA). PLL (poly(L-lysine), P2636) and PEI (poly(ethyleneimine), P3143) were purchased from Sigma-Aldrich (St-Quentin-Fallavier, France). PLL and HA were dissolved to 0.5 mg/ml in HEPES-NaCl buffer (20 mM HEPES at pH 7.4, 0.15 M NaCl), both purchased from Sigma-Aldrich (H4034 and S9625, respectively). For the studies on the 2D substrate, film deposition was performed in a 96-well plate (Greiner, Les Ulis, France) using an automatic liquid robot (EVO100, Tecan, Lyon, France). This robot can automatically aspirate and dispense fluids into multiwell plates, as previously described [36]. Prior the deposit the 12 (PLL/HA) layers pairs, a first anchoring layer of PEI was incubated at 5 mg/ml for 20 min. For 3D studies, the scaffolds were placed in a 24-well plate (662892, Greiner, Les Ulis, France) together with their Ø14 mm glass coverslip. Then, 2.5 mg/ml PEI was added to the wells and incubated under vacuum for 20 min. The robot applied successive layers of PLL and HA until the 12 bilayers were formed. After formation, all films were cross-linked for 18 h at 4 °C with 1-ethyl-3-(3-dimethylamino-propyl) carbodiimide (EDC, E7750) at a concentration of 30 mg/ml or 70 mg/ml and N-hydrosulfosuccinimide (Sulfo-NHS, KRO-12021) at a constant concentration of 11 mg/ml, obtained from Sigma-Aldrich (St-Quentin-Fallavier, France) and Chemrio (Ningbo, China), respectively. Final washing was performed with HEPES-NaCl buffer for 1 h. The films were then dried after a brief rinse with H2O. The multilayer films are hereafter referred to as EDC30 and EDC70, which stand for soft and stiff films, respectively, and refer to the concentration of the cross-linking agent.

Characterization of the polyelectrolyte film-functionalized structure

Both the Ormocomp scaffold and the Ormocomp scaffold functionalized with PEM were characterized using optical and electronic microscopy. Images were acquired using a Zeiss LSM700 confocal scanning microscope (Zeiss, Le Peck, France) equipped with a 63X oil immersion objective and laser diodes at 405, 488, 555, and 639 nm. Images were acquired using the Zen software by Zeiss. In addition, 3D reconstructions of the acquired z-stacks were created using ImageJ software (imagej.nih.gov/ij/). For the observation of the polyelectrolyte film, the last layer was a PLL-FITC layer (Sigma-Aldrich, P3069). For analysis of SEM, the scaffolds were coated with a 20 nm thick carbon layer using the Bal-Tec CED030 carbon filament evaporator (Bal-Tec Union Ltd., Liechtenstein) and imaged with a Quanta 250 field emission gun SEM (FEI Company) at 5 kV with a high contrast backscatter detector.

Protein loading on polyelectrolyte films

Fibronectin (11051407001) was obtained from Roche (Basel, Switzerland), BMP2 from the IndoctOs kit from Medtronic (Minneapolis, USA), and BMP4 (120-05ET) from Peprotech (Neuilly-sur-Seine, France). Proteins were dissolved in 1 mM HCl buffer (258148 from Sigma Aldrich) at pH 3. For studies on 2D substrates, proteins were incorporated into the film for 1h30 at 37°C and then rinsed with HEPES-NaCl buffer. They were then dried after a short rinse with H_2O. For 3D studies on the scaffold, 1 µl of protein solution was applied to the scaffold and incubated for 10 min at RT to allow incorporation. Then the scaffolds were quickly rinsed with H_2O and dried. Incorporation of proteins into the PEM was confirmed with 10% fluorescent BMP2 coupled with rhodamine (prepared in-house) and observed under the LSM700 confocal microscope. To control for proteins bound to the matrix, we also examined the dynamics of cancer cells exposed to soluble proteins added directly to the cell culture media. We will refer to the proteins loaded into the PEM as matrix-bound proteins (bFN, bBMP2, and bBMP4) and soluble proteins (sFN, sBMP2, and sBMP4). The amount of protein loaded into the film was checked using a QuantiPro™ BCA assay (QPBCA, Sigma-Aldrich), and the results are shown in **Table S1**. The stiffness previously measured using the AFM nanoindentation technique was not affected by protein loading[34].

Cell culture and cell seeding on the scaffold

Pancreatic cancer cell line PANC1, derived from epithelioid carcinoma in a 56-year-old man, was acquired from ATCC (CRL -1469). The patient-derived cells PAN092 (CTI-214) were developed by CTI-Biotech (Meyzieu, France), from the French cancer consortium IMODI. PAN092 cell was isolated from a patient's biopsy and propagated in mice as patient-derived xenografts (PDX). It is an invasive and moderately differentiated pancreatic ductal carcinoma (G2) of the pancreatic head were cultured in DMEM-F12 supplemented with 10% FBS (10270-106) and 1% Antibiotic-Antimycotic

(15240-062) (all from Thermo Fisher Scientific, Bourgoin-Jallieu, France) and maintained at 37°C and 5% CO_2. All substrates (plates and scaffolds) were sterilized under UV light for 20 min before seeding the cells. For the 2D studies, cells were seeded at a cell density of 15,000 cells/cm². In the 3D cell culture, cells were seeded at 32,000 cells per scaffold. Cells were seeded in 1 µl on the top of the scaffold, with 1 µl of medium added periodically to prevent desiccation. The wells were filled with medium once the cells were attached to the scaffold after approximately 1 hour.

High content imaging and quantification of cell adhesion and spreading

Cell adhesion and spreading were analyzed after 16 h for PANC1 cells and after 24 h for PAN092 cells due to their low adhesion rate. Cells were fixed with 3.7% paraformaldehyde (252549 from Sigma-Aldrich, Saint-Quentin Fallavier, France) for 20 min. The actin cytoskeleton of the cells was stained by incubation with phalloïdine rhodamine (P1951, from Sigma Aldrich) for 30 min. Cell nuclei were stained by 5-minute incubation with DAPI (D9542, from Sigma Aldrich). Automated imaging was performed using a high-content imager GE InCell 2500 (General Electric, Buc, France) equipped with 4X, 10X, and 20X air objectives. Bright field images were acquired with a 4X objective. Fluorescent cell images were acquired with the 10X objective in eight fields to cover most of the well. Automated analysis was performed using the manufacturer's GE IN-Carta software (General Electric, Buc, France). The cell count indicates the average number of nuclei counted in 1 mm² of the well surface. Cell spread corresponds to the cell area labeled with phalloïdine rhodamine (targeting the cytoplasm of the cells). Each experiment was performed at least in triplicate, with three independent samples per condition in each experiment. The average cell number per mm² or the average cell area (µm²) was plotted along with the SEM.

Cell proliferation assay

To assess the proliferation of PANC1 and PAN092 on the 2D substrate, cells were cultured on a polyelectrolyte film with increasing concentrations of bFN, bBMP2, and bBMP4. Cells were lysed and processed using the CyQUANT assay (C7026, Thermo Fisher Scientific) according to the manufacturer's protocol at 38, 76, 114, and 152 h for PANC1 cells and 24, 48, 72, 96, and 120 h for PAN092 cells. Fluorescence was detected using a plate reader (Infinite1000, Tecan, France) with an excitation wavelength of 480 nm and an emission wavelength of 520 nm. All experiments were performed at least in triplicate (i.e; three independent experiments) with three independent samples per condition in each experiment, and the average $\pm$ SEM was plotted.

pSMAD analysis

For analyzing pSMAD1/5/9, cells were fixed 5 h after seeding to allow adhesion. After fixation and membrane permeabilization, the cells were blocked using 3% w/v BSA (A4503, Sigma-Aldrich, Saint-Quentin Fallavier, France) in PBS. Next, the primary antibody anti-pSMAD1/5/9 (13820S, Cell Signaling, Leiden, Netherlands) was diluted in the ratio of 1:400 in the 3% BSA solution and incubated overnight at 4°C. After overnight incubation, the plates were washed 3 times with PBS to remove an attached primary antibody and then incubated with the fluorescently tagged secondary antibody (A32732, Invitrogen, Paris, France) at room temperature for 1 h. The images were analyzed using GE INCA 2500 (General Electric, Buc, France) imaging system using a 20X objective. Up to 1000 cells were analyzed in each condition for three independent experiments, and graphs were plotted on Origin software with the average pSMAD signal and SEM.

Statistical analysis

Statistical comparisons were performed using OriginPro software version 2020b. The nonparametric Bonferroni test was used to analyze data from two independent groups. ANOVA, followed by an appropriate pairwise comparison or comparison with the control group, was performed ($p<0.05$ was considered significant). All experiments were repeated at least 3 times with at least two samples per condition in each experiment. The error bars represent the standard errors of the mean. The asterisk indicates that the value is significantly different from the control condition.

Results

Fabrication of the 3D Ormocomp scaffold

The details of the structure and scaffold design, which was created using computer-aided design software, are shown in **Figure 2.A-B**. Scaffolds with three different porosities (80 µm, 100 µm, and 120 µm) were fabricated and analyzed using optical microscopy. These different porosities were chosen to allow cell-cell contact, nutrient exchange, and proliferation in the structure[35]. The bright-field image of the top of the bare scaffold **(Figure 2.C)** and the 3D reconstruction **(Figure 2.D)** show that the Ormocomp scaffold is compatible with any optical microscopy analysis technique due to its transparency. The scanning electron micrographs show that the scaffold was fabricated without defects **(Figure 2.E)**. The roughness of the scaffold surface **(Figure 2.F)** can be adjusted by increasing or decreasing the laser power and writing speed[36]. Initially, a photo-initiator was added to Ormocomp to improve the polymerization process. However, it caused undesirable autofluorescence and led to the destruction of the scaffold during UV sterilization (data not shown). In addition, photo-initiators are known to exhibit some cell toxicity[37]. Due to these problems, the scaffolds were prepared without this additional photo-initiator. An advantage of the Ormocomp scaffold is that they did not show swelling compared to natural polymers[38].

ծ

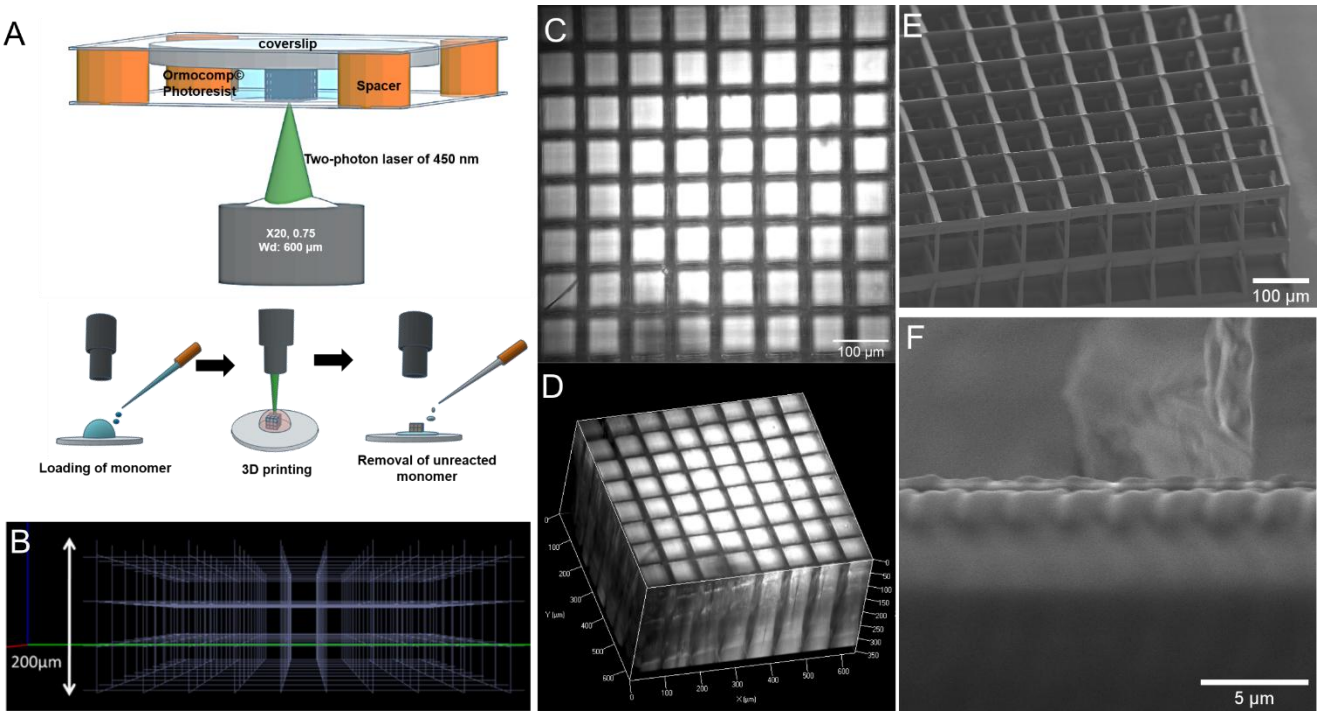

Figure 2. Fabrication and characterization of the 3D Ormocomp scaffold. (A) Structure and steps in TPP, **(B)** with the computer-aided design. Optical image in bright field **(C)** of the top view and **(D)** 3D reconstruction. Scanning electronic microscope (SEM) images of **(E)** the scaffold and **(F)** its surface.

Film buildup and protein incorporation on the 3D scaffold

Due to the low interaction between Ormocomp and cells[39], it is crucial to apply an additional coating on the scaffold surface that mimics the ECM[40] to allow cell culture and colonization inside the 3D structure. Three different scaffold pore sizes (80, 100, and 120 µm) were tested, and the PEM film coating was characterized by fluorescence microscopy. PLL-FITC was used for the visualization of the film[27]. Fluorescence microscopy showed that increasing the pore size leads to a uniform coating of the PEM film on the scaffold **(Figure S1**). This uniform coating is mainly due to reduced surface tension and facilitated fluid exchange due to larger pores during successive layer deposition. Therefore, we selected the scaffold with a pore size of 120 µm for further experiments.

PEI was precoated on the scaffold as a anchoring layer to improve the deposit of polyelectrolytes: PEI has excellent UV resistance, transparency, mechanical stability, and good biocompatibility[41]. In the absence of this first PEI layer, the film was not uniformly deposited on the scaffold **(Figure S2)**. Due to the hydrophobicity of the Ormocomp material, incubation was performed under vacuum to enable liquid impregnation into the structure. The confocal fluorescence images at high magnification (63X) showed a uniform coating of ~ 1.5 µm on the hydrated scaffold **(Figure 3.A-B)**, which is previous quantification of film thickness[30]. The microscopic size of this 3D scaffold being fully compatible with the protocols already established for the polyelectrolyte films in 2D, similar

protocols were used to visualize labelled films and proteins. Rhodamine-labelled BMP2 was loaded into the film-coated scaffold and then imaged using confocal microscopy **(Figure 3.C-D)**. The uniform red staining around the scaffold bars shows the homogeneous incorporation and distribution of the protein within the film.

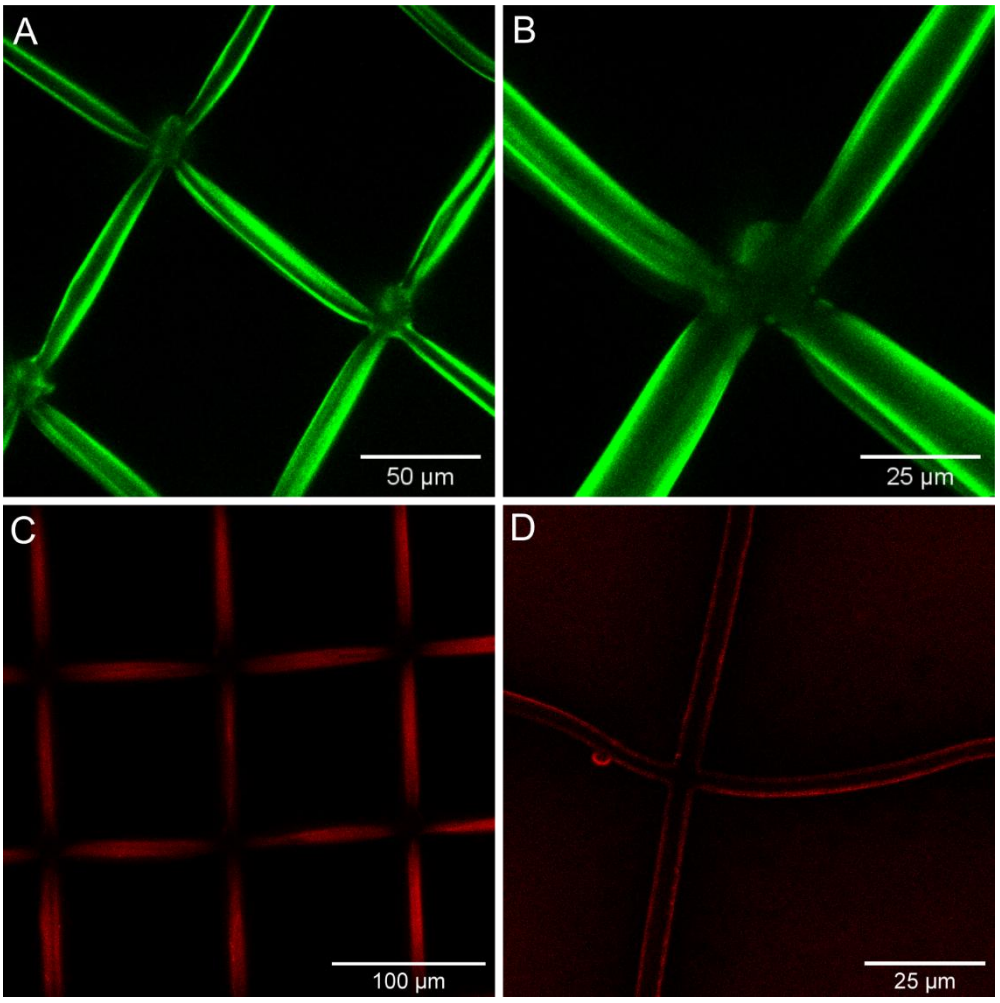

Figure 3. Characterization of the coated 3D PEM-Ormocomp structure and of protein loading on the scaffold using a confocal scanning microscope. PEM coating labelled with PLL-FITC (green) **(A, B)** and BMP2 rhodamine (red) on the hybrid structure **(C, D)**.

Pancreatic cancer cell line on PEM film-loaded with FN, BMP2, and BMP4

To design an optimal 3D microtumor model, it is essential to know how signaling molecules affect basic processes such as adhesion, spreading, and proliferation of cells on PEM film[42]. It is also known that film stiffness affects the interaction between cancer cells and the matrix-bound biomolecules. We studied these processes on soft (EDC30) and stiff (EDC70) films. Moreover, the extracellular matrix proteins play an important role in cell dynamics and cancer cell survival[43]. To construct the successful 3D microtumor model, we investigated the effects of the bioactive film loaded

with the selected proteins (FN, BMP2 and BMP4) on the two pancreatic cancer cell lines PANC1 and PAN092.

PANC1 response to matrix-bound FN, BMP2, and BMP4

The PANC1 cell line, established from pancreatic ductal carcinoma, is a widely used model of pancreatic cancer and is well characterized. As previously mentioned, adhesion proteins and growth factors significantly influence cellular processes such as cell adhesion, spreading, and proliferation. PANC1 cells cultured on TCPS showed higher cell adhesion, spreading, and proliferation than control films EDC30, EDC70 **(Figure S3)**. The proliferation assay showed that the cells grew linearly on TCPS for up to 160 h. Cell proliferation was higher than that of the control films. This increased proliferation may be due the physico-chemical properties of TCPS to improve cell attachment. EDC30 is also known as a soft film due to its low stiffness. When cultured on EDC30 and EDC70 films, the cells are round and often observed as clamped with each other **(Figure S3.A-B)**. In addition, cell spreading was lower on EDC30 films **(Figure S3.C)** since a softer substrate allows less interaction between the cell adhesion receptors integrins and the underlying matrix. This lower adhesion favors cell-cell interactions instead of cell-substrate interactions[44], and also to a lower proliferation rate than that on TCPS **(Figure S3.D)**. On EDC30 and EDC70, cells proliferated slightly within 80-120 h, and after 120 h, the cell population decreased. At 120 h, PANC1 cells aggregated and formed organoid-like aggregates on EDC30 and EDC70 films **(Figures S4 and S5)**.

As a control, we added the soluble proteins on cells cultured on TCPS and analyzed cell adhesion and spreading for both cell lines. For the PANC1 cell line, only fibronectin had an effect on cell adhesion and spreading **(Figure S6)**. In PAN092 cells, the proteins had no significant effect on cell attachment, but also had no effect on spreading **(Figure S7)**. Next, we examined the above effect of the proteins in soluble form (sFN, sBMP2 and sBMP4) and matrix-bound form (bFN, bBMP2 and bBMP4) in EDC30 and EDC70. bFN highly promoted adhesion and proliferation of PANC1 cells on both EDC30 and EDC70, but had no effect on cell spreading **(Figure 4.A-E)**. The corresponding fluorescence images are shown in **Figures S8 and S9**. When a minimal amount of bFN (2.5 µg/ml) was added to the EDC30 film, cell adhesion increased dramatically. The number of attached cells was about 100 per mm², and when 2.5 µg/ml of bFN was present in the film, the cell number increased 5-fold for cells on EDC30 and 15-fold for EDC70 films **(Figure 4.C)**. This significant increase in cell attachment indicates that bFN provides binding sites for PANC1 cells. Interestingly, sFN had no effect on cell adhesion for cells on EDC30 films **(Figure S6.A)**. Indeed, fibronectin increases cell adhesion by interacting with integrins at the cell surface[45].

The proliferation of PANC1 cells was analyzed using a cyQUANT assay. PANC1 cells proliferated on both EDC30 and EDC70 films loaded with bFN **(Figure 4.E)**. In contrast, bBMP2 and

bBMP4 showed a much milder effect on cell adhesion, with a dose-dependent increase on cell adhesion **(Figure 4.F and 4.I)**. They did not induce cell spreading **(Figure 4.G and 4.J)**, with here again no distinction between soft and stiff films. However, this may be explained by the epithelial-like nature of pancreatic cells. Indeed, epithelial cells remain morphologically compact and therefore did not spread even when under favorable conditions. Both sBMP2 and sBMP4 showed no effect on the adhesion of PANC1 to TCPS **(Figure S6.C and S6.E)**. Although bBMP2 and bBMP4 slightly increased cell adhesion, they did not affect cell proliferation, except for the lowest bBMP2 concentration (5 µg/ml), regardless of film stiffness **(Figure 4.H and 4.K)**. The cell population is relatively stable and begins to decrease after 114 h for bBMP2. Finally, bBMP4 had no effect on cell proliferation except at the highest concentration on soft films, where the cell number increased significantly after 160 h **(Figure 4.K)**.

Overall, we found that the number of attached cells was lower on EDC70 films in the presence of matrix-bound proteins than on EDC30 loaded with the same proteins. This indicates that the combination of soft films with matrix-bound proteins (bFN, bBMP2, and bBMP4) provided more favorable conditions for PANC1 cell attachment. This suggests that adhesion of PANC1 cells depends on film stiffness independently of the proteins presented. On the other hand, sFN, sBMP2 and sBMP4 show similar trends for cells cultured on slide **(Figure S10)**. However, the number of attached cells in the presence of soluble proteins was lower than with matrix-bound matrix. BMP2 and BMP4 are known to promote epithelial to mesenchymal transition by limiting cell adhesion and proliferation[18]. This was confirmed by the proliferation inhibitory role of BMPs on pancreatic cancer cells, as already highlighted in the literature[46]. After 120 h, PANC1 cells aggregated and formed organoid-like aggregates in bFN, bBMP2 and bBMP4 on EDC30 and EDC70 **(Figures S4 and S5)**. This cellular morphology confirms that the bioactive film mimics the ECM by allowing cells to self-organize, to aggregate and form colonies. When the concentration of bFN increased, we obseved that this organoid morphology was disrupted, with cells being mostly present as single cells. At the same time, the organoid morphology on both bBMP2 and bBMP4 was similar to the control at all concentrations. To note, we did not observe this organoid morphology with sFN, SBMP2 and sBMP4 (data not shown).

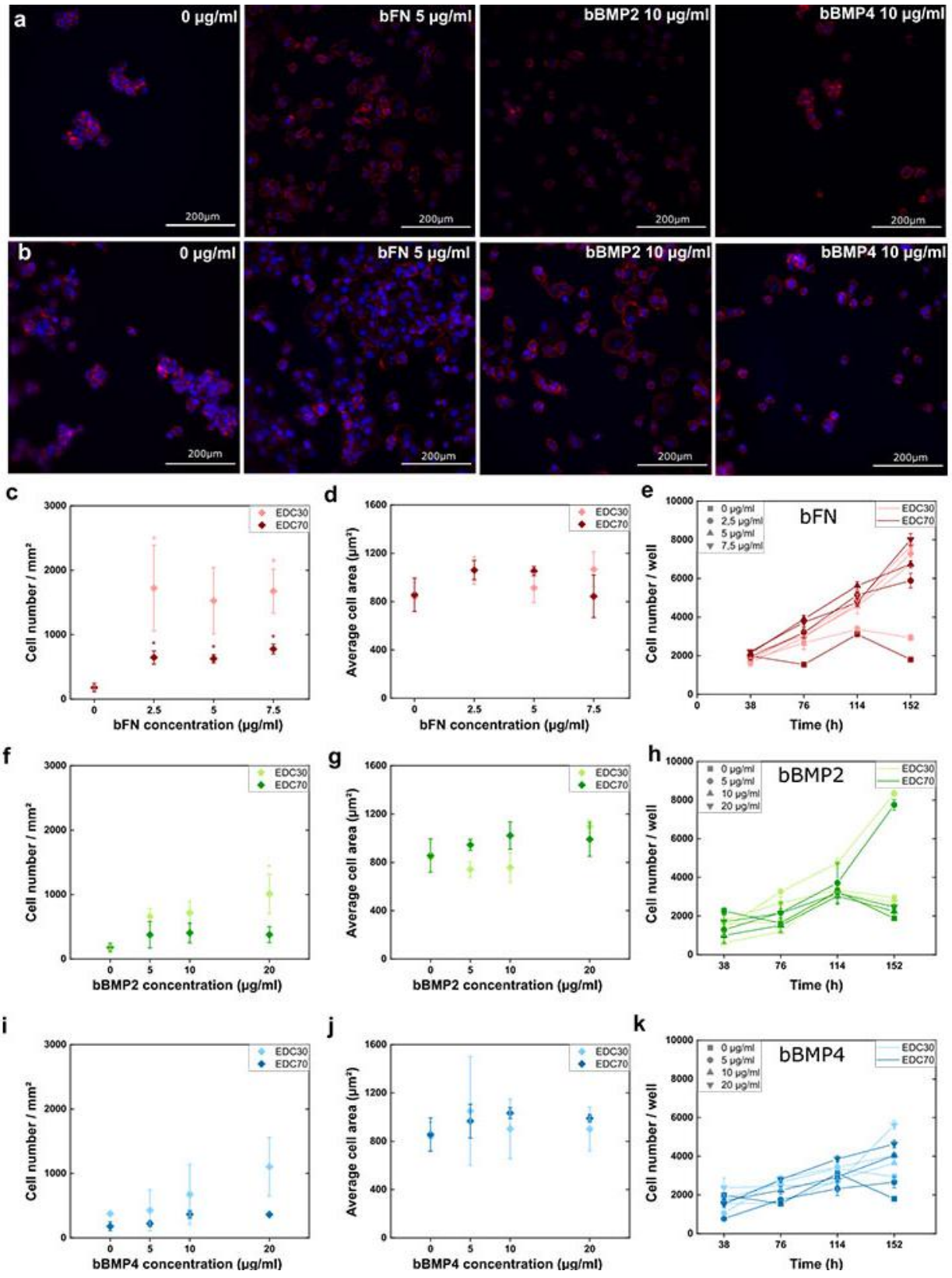

Figure 4. Cell adhesion, spreading and proliferation of PANC1 on soft (EDC30) and stiff (EDC70) PEM film. Fluorescence images of cells with nucleus labelled with DAPI (blue) and actin cytoskeleton labelled with rhodamine (red) on **(A)** soft film and **(B)** stiff film with FN, bBMP2 or bBMP4. Cell adhesion

(C, F, I), cell spreading **(D, G, J)**, and proliferation **(E, H, K)** were quantified in the presence of fibronectin (C-E), BMP2 **(F-H)**, or BMP4 **(I-K)**. The mean of 3 independent experiments is plotted with SEM. * indicates that the value is significantly different from the control condition.

PAN092 response to matrix-bound FN, BMP2, and BMP4

To compare the results of the immortalized cell line (PANC1) with those of the patient-derived cells (PAN092), a similar experiment was performed **(Figure 5)**. CTI-Biotech maintains these cells as part of the IMODI Cancer Consortium, and the cells were dissociated from a patient-derived pancreatic tumor xenograft. The cell line PAN092 was isolated from an invasive but moderately differentiated pancreatic ductal carcinoma of the pancreatic head. Interestingly, the number of cells was higher on EDC70 than on TCPS and EDC30 **(Figure S11.A-B)**. Importantly, proliferation was also slower than PANC1 cells, but similar to TCPS, EDC30 and EDC70, as expected for a patient-derived tumor population **(Figure S11.D)**. On both soft and stiff films, bFN strongly increased adhesion of PAN092 cells, even at the lowest dose of 2.5 µg/ml **(Figure 5.C)**. bBMP2 showed a gradual increase in adhesion in a dose-dependent manner from 5 to 20 µg/ml, but it was significant only for the lowest dose loaded into the stiff film **(Figure 5.F)**. In contrast, bBMP4 had a negative effect on adhesion to stiff films at the highest dose **(Figure 5.I)**. We also found stiffness-dependent adhesion for bBMP2 and bBMP4, but unlike PANC1, PAN092 cells seemed to prefer stiffer film. Cell spreading was very similar to PANC1 cells and was not affected by the loaded proteins and stiffness, except for the highest dose of bFN on EDC30 **(Figure 5.D, 5.G, 5.J)**. bFN slightly increased cell proliferation, while bBMP2 and bBMP4 had no significant effect **(Figure 5.E, 5.H, 5.K)**. On the other hand, sFN, sBMP2 showed an increase in cell attachment on TCPS and EDC30 **(Figures S12, S13)**. sFN and sBMP2 showed no effect on EDC70 **(Figures S12, S13)**. sBMP4 showed the opposite effect than bBMP4 on TCPS, EDC30 and EDC70 **(Figures S7.E and S13.E)**.

bBMP2 and bBMP4 did not affect PAN092 proliferation, regardless of film stiffness. This was consistent with the proliferation inhibitory role of BMPs on pancreatic cancer cells reported in the literature[47]. Nevertheless, these patient-derived PAN092 cells showed specific differences from the ATCC cell line PANC1. Overall, PAN092 proliferated two time slower than PANC1. This may be explained by the non-immortalization of the cell line compared to immortalized established cell lines and its low adhesion rate, which remains a particular stumbling block in pancreatic cancer research[48]. There was stiffness-dependent cell adhesion in both cell lines, but, unexpectedly, PANC1 and PAN092 responded in opposite ways. In fact, PANC1 cells preferred a softer film regardless of the matrix-bound protein, while PAN092 preferred stiffer films. bFN appeared to override this stiffness-dependent adhesion of PAN092. This may be explained by the presence of RGD motifs in the protein, being a strong adhesive signal for the cells by interacting with the adhesion receptors integrins[49].

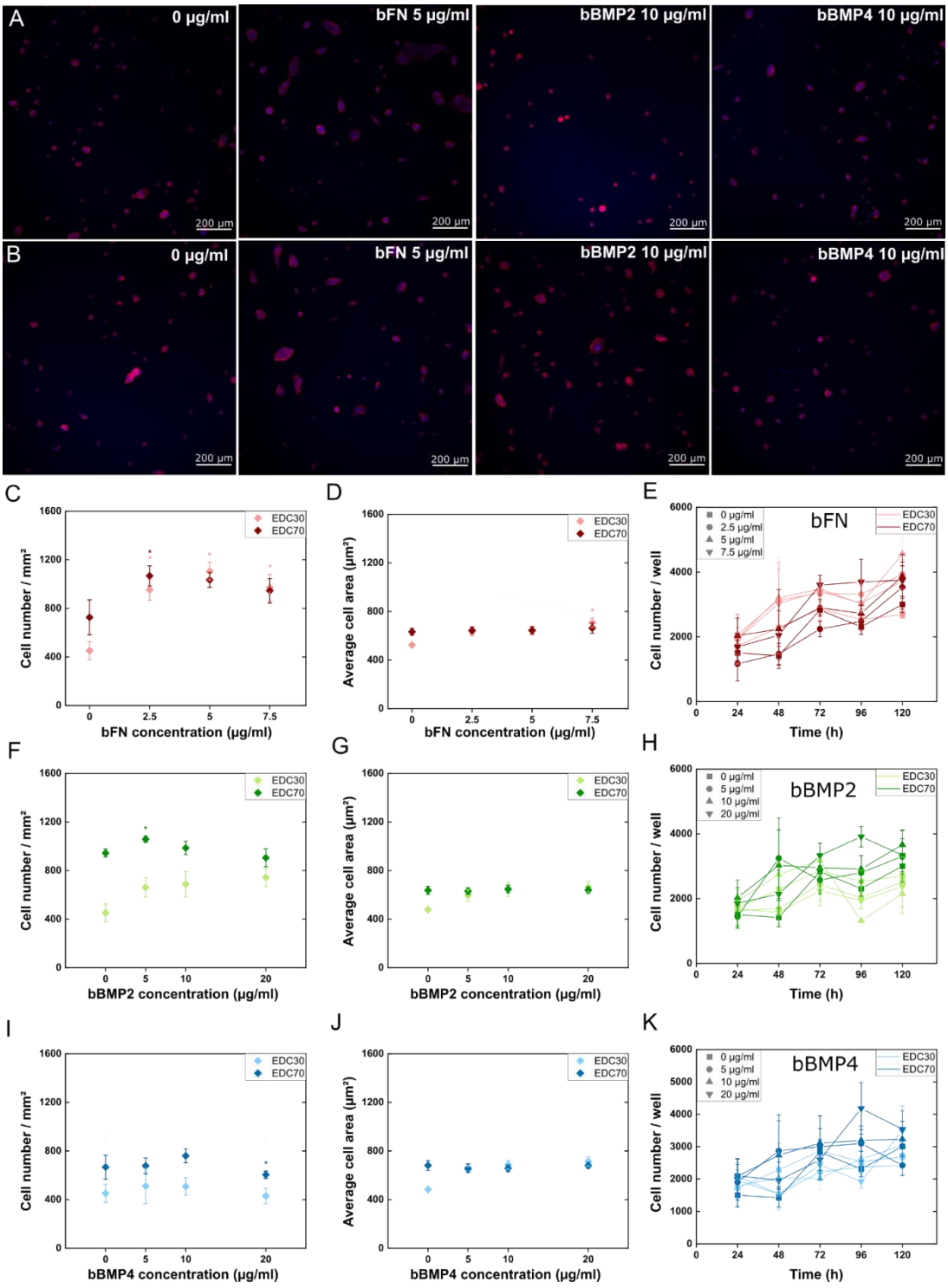

Figure 5. Cell adhesion, spreading and proliferation of PAN092 on soft (EDC30) and stiff (EDC70) PEM film. Fluorescence imaging of cells with nucleus labelled with DAPI (blue) and actin cytoskeleton labelled with rhodamine (red) on **(A)** soft film and **(B)** stiff film with FN, BMP2 or BMP4. Cell adhesion (**C, F, I),** cell spreading **(D, G, J),** and proliferation **(E, H, K)** were examined in the presence of fibronectin **(C-E)**, BMP2 **(F-H),** or BMP4 **(I-K).** The mean of 3 independent experiments is plotted with SEM. * indicates that the value is significantly different from the control condition.

Bioactivity in response to the matrix-bound proteins in the films

To further investigate the effect of proteins on cellular processes, we assessed the cell response to BMPs via the Smad signaling pathway. Upon interaction of BMP with its receptor at the cell surface, a signaling cascade is triggered in which Smad1/5/9 is phosphorylated. We quantified the phosphorylated form of Smad1/5/9 using immunofluorescence **(Figure 6)**. For PANC1 cells **(Figure 6A-E)**, we observed that there was no pSMAD signal on films with bFN whatever their stiffness. This is consistent with the fact that fibronectin is an adhesion protein that interacts with integrins and not with BMP receptors. However, the pSMAD in response bBMP2 and bBMP4 showed a strong increase for both EDC70 and EDC30 films **(Figure 6.A-E)**. For PAN092 cells **(Figure 6.F-J)**, we did not detect a pSMAD response whatever the bBMP concentration. Thus, PAN092 cells did not respond to BMPs via the Smad signaling pathway. The same proteins administered in soluble form showed the same trends for both cell lines, but with a lower pSMAD intensity **(Figure S15)**. This increased effect of matrix-bound proteins may be related to the increased protection of the proteins from aggregation and conformational changes, and the presentation of the proteins at the ventral side of the cell is also more physiological[50]. The effects of the proteins on the different cellular processes are summarized in **Table 1**.

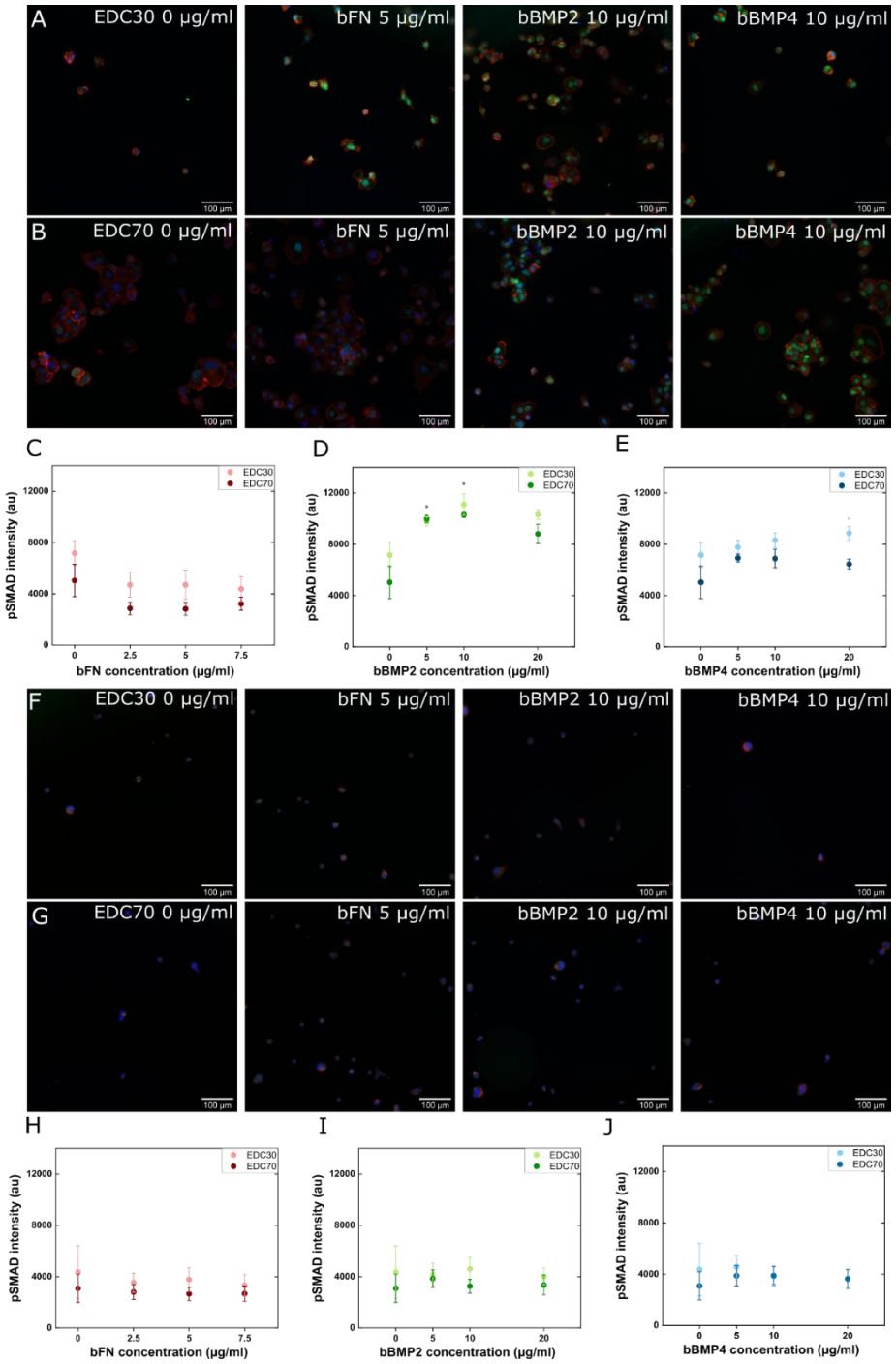

Figure 6. pSMAD signaling of PANC1 and PAN092 on soft (EDC30) and stiff (EDC70) PEM film. Fluorescence images of PANC1 cells on **(A)** EDC30 and **(B)** EDC70 and PAN092 cells on **(F)** EDC30 and **(G)** EDC70, with the nucleus marked in blue, the actin cytoskeleton in red, and pSMAD1/5 in green. The intensity of the fluorescent signal from pSmad1/5 was measured **(C-E)** in PANC1 cells and **(H-J)** in PAN092 cells on EDC30 or EDC70 in the presence of bFN, bBMP2, or bBMP4. The average intensity of the signal was plotted along with the SEM. * indicates that the value is significantly different from the control condition.

		bFN	bBMP-2	bBMP-4
PANC-1 EDC30	Adhesion	+++	+ dose-dependent	+ dose-dependent
	Spreading	=	=	=
	Proliferation	+++	++++ low dose = high dose	++ dose-dependent
PANC-1 EDC70	Adhesion	++	=	=
	Spreading	=	=	=
	Proliferation	+++	++++ low dose = high dose	++ high dose + low dose
PAN092 EDC30	Adhesion	+++	+ low dose = high dose	- dose-dependent
	Spreading	+ dose-dependent	=	=
	Proliferation	++	--	=
PAN092 EDC70	Adhesion	+++	=	=
	Spreading	=	=	=
	Proliferation	+	~+	~+

Table 1. Table summarizing the effects of the matrix-bound proteins on the different cellular processes, including cell adhesion, spreading, and proliferation, for the two cell types: PANC1 cell line and PAN092 cells on stiff or soft films with matrix-bound bFN, bBMP2 and bBMP4. The '+', '++', "+++" and "++++" indicate an increasing level of positive effects, while "-" and "--" indicate a negative effect on the process. "=" indicates that there is no effect on the process

3D cell culture on functionalized scaffolds

To combine scaffold functionalization with cell culture on planar films, cancer cells were cultured on the 3D functionalized scaffolds coated with the protein-loaded films. We followed and studied their growth and proliferation over 20 days. Initial results for these cell cultures in 3D are shown in **Figure 7**. Long-term 3D culture of PANC1 cells on fibronectin-loaded soft sheets was followed for up to 21 days by optical imaging **(Figure 7.A)**. After 20 days, a colonization of the scaffold was observed from bottom to top and the formation of a compact cell mass. After 11 days, the nuclei and cytoskeleton were stained to highlight cell colonization inside the scaffold **(Figure 7.B)**. Cells were present between the scaffold bases, demonstrating vertical colonization by PANC1 cells. In addition, a Live and Dead assay

with live cells in green and dead cells in red, was performed after 20 days of culture **(Figure 7.C)**. A very high viability of the cells was found within the cell aggregates. No necrotic core was visible in the cell mass. These data provide a first insight into 3D cell culture within the functionalized scaffolds.

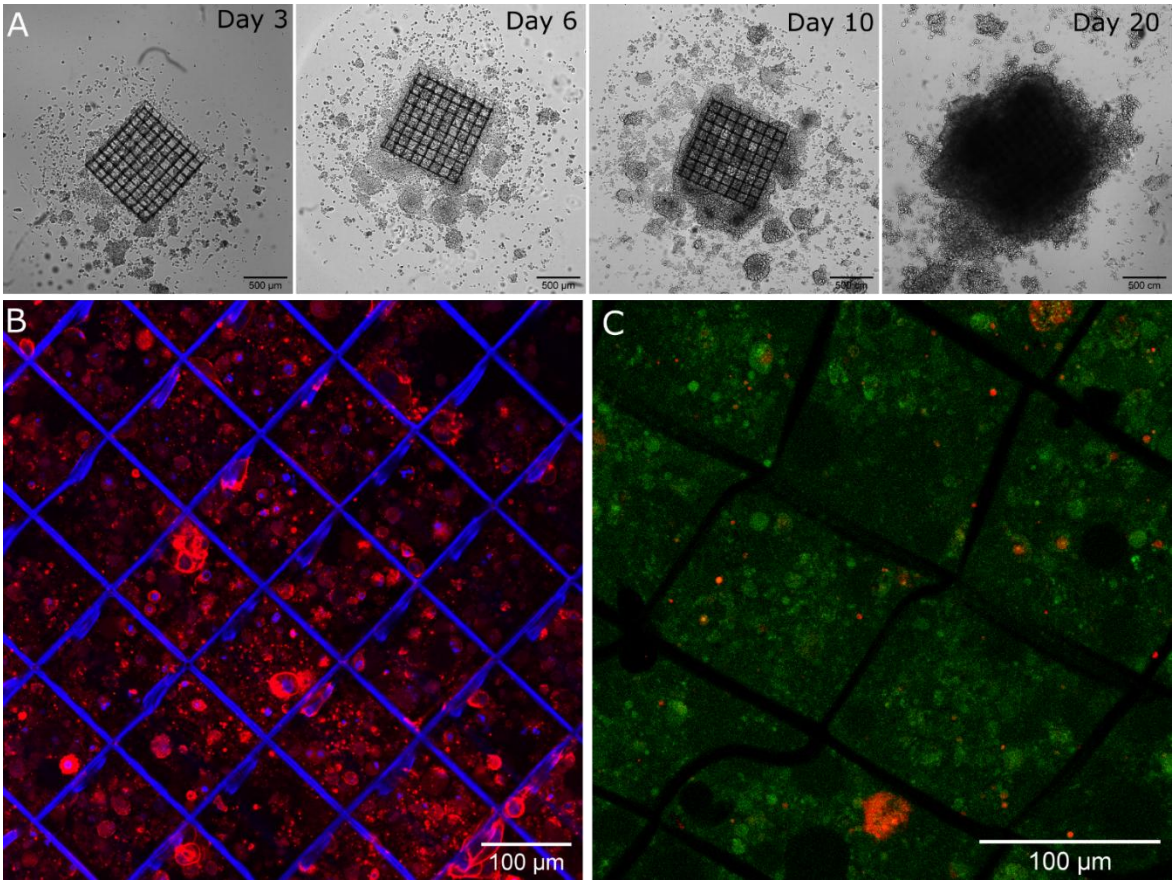

Figure 7. 3D culture of PANC1 cells on the bioactive scaffold loaded with 5 µg/ml fibronectin. (A) Bright field images of cells after 3, 4, 10 and 20 days of culture. Confocal images of PANC1 cells **(B)** with nucleus stained blue (DAPI) and cytoskeleton stained red (rhodamine) after 11 days in culture and **(C)** Live & Dead assay after 20 days in culture with live cells labelled in green and dead cells labelled in red.

Discussion

Tissue architecture and physicochemical conditions are essential factors in the development of a successful tumor model. The polyelectrolyte multilayer can mimic the biomechanical conditions of the ECM. Lin et al. showed that polyelectrolyte multilayer films made of chitosan and heparin could deliver TGFβ to monocultures of primary human hepatocytes (PHHs) PHH/non-parenchymal cells (NPC). They also found that delivery of soluble TGFβ downregulated PHH function, while delivery of bound TGFβ resulted in upregulation of PHH functions in 3 out of 4 cases[51]. Our team previously reported the

fabrication of various types of polyelectrolyte multilayer films mimicking the ECM. We have studied the cellular dynamics in detail using different signaling molecules and several cell lines cultured on different PEM films[50,52,53]. In the present work, we studied the adhesion and growth of pancreatic cancer cells (PANC1 and PAN092) on PEM and proved that bioactive PEM can be successfully deposited on 3D Ormocomp scaffold. Advantageously, this approach may be applied to various polymers, ceramics and composites. In a tumor, the stiffness of the ECM is continuously adjusted to ensure the survival of cancer cells. The present approach enables to independently control and tune the 3D scaffold architecture and the 2D biomimetic films coatings, notably its stiffness and the type of loaded proteins (ECM or growth factor), in order to mimic the tumor microenvironment in a simplified and well-controlled manner. We also address another critical problem, regarding protein aggregation and the burst release of proteins from 3D scaffolds. Indeed, the PEM-functionalized Ormocomp structure is stable under cell culture conditions for extended periods of time without mechanical damage or swelling problems.

In most 3D-printed materials, proteins are adsorbed directly on the surface, leading to a burst release during cell culture[54]. Microtumor generation with the TPP has significant advantages[55] over available 3D cancer models such as organoids based on passive movement into a scaffold and spheroids based on passive accumulation due to limited direction of culture pathways. The femtosecond laser uses a nonlinear process to create a free-standing 3D structure. Various natural polymers (e.g., collagen, dextran, fibrin, and chitosan), their combination (e.g., collagen-acrylate, alginate-acrylate), and ceramics can be used in TPP[56]. Natural polymers, such as collagen, are interesting in that they mimic the ECM, but conversely, they naturally induce various signaling pathways in cancer cells. In addition, using natural polymers may need high levels of crosslinking agents or photo-initiators, which can have toxic effects on cancer cells[57]. Ormocomp is an inert and biocompatible polymer, which is photosensitive and enables high-resolution polymerization when exposed to a specific wavelength[58]. Ormocomp-based 3D models have been much discussed in recent research because of their biocompatibility, excellent transparency, and higher mechanical and chemical stability[40]. The use of TPP and the low refractive index of Ormocomp (1.520) allowed the scaffold to be fabricated without defect at submicron resolution. Thanks to its inertness, it does not trigger cell signaling pathways, unlike collagen-based hydrogels. However, the drawback is precisely that it needs further surface modification [40]. This is possible in view of the fact that it is a silicate-based organic-inorganic composite[36]. The roughness of the Ormocomp framework facilitates the adsorption of polyelectrolytes on the surface. Thus, surface functionalization via the biomimetic layer-by-layer films containing ECM proteins and growth factors can be advantageously used to provide bioactive signals. The automation of the LbL deposit process ensures an excellent reproducibility in the surface coating of the 3D scaffold. (**Figure 2**). Altogether, the automated fabrication process and functionalization of the Ormocomp 3D structure ensured a high precision and robustness for large-scale preclinical *in vitro* studies. We noted that mechanical stability was good over time and that long-term cell culture was

possible. We found that cell adhesion was enhanced after coating the scaffold with the PEM film loaded with FN. This is consistent with previous results showing that TU scaffolds coated with fibronectin enabled long-term cell culture[9]. Furthermore, we showed that cells can remain in culture for at least 20 days in the 3D scaffold, which is important and will enable future long-term drug testing.

We have previously reported the uniform loading of BMP2 in PEM film[27]. Here, using fluorescence confocal microscopy, we showed that protein loading in the film-coated 3D Ormocomp structure was uniform. Micro-BCA analysis confirmed that the three proteins (FN, BMP2 and BMP4) were loaded in the film at ~80 to 90% efficiency.

Here, we studied two types of pancreatic cancer cells, a model cell line PANC1 and a patient-derived cell line PAN092, both with a similar number of passages (< 14). PANC1 cells are known for their aggressive growth[59], while PAN092 showed slower growth than PANC1. PANC1 cells showed significant stiffness-dependent adhesion and preferred softer substrates. In contrast, PAN092 adhered more to the stiff EDC70 film than to EDC30 ones. The proliferation of PANC1 and PAN092 cells was similar on EDC30 and EDC70 films. In TCPS, PANC1 cells proliferated in an exponential phase even after 120 h. However, on EDC30 and EDC70 films, cell proliferation slowed down after 120 h and we observed an organoid-like morphology of cell aggregates in the film. Conversely, PAN092 cells grew in a steady state over the 5 days of culture and showed a similar morphology. These organoid-like cell assemblies proved that PEM properly supports and maintains the cells to allow 3D expansion. Picollet D'hahan et al. observed a small accumulation of cancerous epithelial prostate cells (PC3) on the polyelectrolyte films, which they explained by the fact that PEM reduces cancer cell migration[60].

We analyzed the effect of signaling molecules, e.g. matrix-bound FN, BMP2 or BMP4 on cancer cells, and compared to their soluble form[61,62]. We found that the number of adherent cells in the presence of matrix-bound protein was higher than for cells in contact with soluble proteins. bFN had a similar effect on PANC1 and PAN092 cells, increasing cell adhesion and proliferation for EDC30 and EDC70 films, independently of film stiffness. We found that twice as much PANC1 cells adhered to EDC30 film than to EDC70 films, even if the amount of FN was similar for both EDC30 and EDC70 films. The increased adhesion induced by FN is consistent with cell adhesion being triggered by integrins[45,63]. Conversely, when fibronectin was added as soluble molecule, it inhibited cell adhesion. bFN increased PANC1 and PAN092 cell proliferation. It has reported that FN enables the continuous proliferation of cancer cells by inhibiting pro-apoptosis pathways through activating FAK and decreasing cytochrome release[64]. Although bFN boosted PAN092 proliferation, the rate was still lower compared to PANC1 cells. We also observed that bFN reduced the organoid nature of the tumor and allowed a more homogeneous distribution of cells inside the culture wells.

Regarding BMP2, bBMP2 slightly enhanced cell adhesion for both cell lines, regardless of film stiffness. However, sBMP2 showed only a minor inhibition of adhesion for both PANC1 and PAN092 cells. Although bBMP2 induced a small increase in adhesion, at higher concentrations (10-20 µg/ml) it had almost no effect on PANC1 cell proliferation whatever the film stiffness. In patient-derived PAN092 cells, bBMP2 had a dual effect on cell proliferation: having no effect for cell proliferation on soft films, while enhancing cell proliferation on stiff films. Here, we observed that bBMP2 inhibited proliferation of PANC1 cells at higher concentrations (10-20 µg/ml) and slightly increased proliferation at low concentrations (5 µg/ml) at both stiffness levels (**Figure 4**). Previous literature highlighted the effect of BMP2 on cancer cell signaling via the Smad pathway. Voorneveld et al.[65] classified cell lines as Smad-positive when BMP2 inhibited proliferation and Smad-negative when BMP2 promoted cell proliferation. In addition, BMP2 was shown to inhibit proliferation of pancreatic cancer cell lines via the Smad pathway[66,67]. Previous studies also revealed the effects of ECM stiffness on Smad signaling pathway. The above results show that film stiffness is very important in the control of Smad signaling in pancreatic cancer.

Regarding bBMP4, it improved both cell adhesion and proliferation of PANC1 cells. However, sBMP4 showed little inhibition of PANC1 cell adhesion. This result also highlighted the importance of film stiffness and delivery mode in the regulation of cell adhesion, spreading and proliferation. However, for PAN092 cells, bBMP4 on EDC30 films inhibited both cell adhesion and proliferation. On stiff EDC70 films, bBMP4 also inhibited of cell adhesion. The above results highlight the bipolar effect of bBMP4 on cancer cells. Virtanen et al. observed that BMP4 significantly reduced cell proliferation in PANC1 and HPAF-II cells by arresting cell growth in the G1 phase [61]. They also observed that MIA PaCa-2 cells did not respond to BMP4. In our work, bBMP4 slightly increase PANC1 cell proliferation on both EDC30 and EDC70 films. For PAN092 cells, the reverse was observed, with an increase in cell adhesion in response to both sBMP4 and bBMP4.

An interesting aspect is the differential pSMAD response for PANC1 cell versus PAN092 cells, PANC1 being BMP responsive notably with sBMP2 and bBMP2, while PAN092 did not respond to BMPs. BMP2 interactions with BMP receptors are the initial steps of the BMP signaling response, which was recently quantified using biolayer interferometry[68]. The fact that PAN092 were insensitive to BMPs may be due to a mutation of Smad proteins that is common in pancreatic cancer[69]. In terms of sensitivity to different BMPs, we observed an increase in pSMAD signaling for bBMP4, but of lower intensity than in response to bBMP2. We also noted that pSMAD response was systematically higher for cells on soft films with bBMPs (**Figure 6**). Regarding FN alone, we found that it did not induce pSMAD signaling and even decreased the pSMAD background. PANC1 grown on FN-coated films were more responsive to sBMP2 on soft films, while PAN092 were more responsive to sBMP2 on stiff films (**Figure S15**). In a previous study, we showed that myoblast cells cultured on FN micropatterns can modulate the BMP

response[70]. Interestingly, our results demonstrated that the combination of the presentation of signaling molecules and film stiffness can affect cancer cell phenotype, proliferation, and the signaling cascade.

Overall, we showed that engineered biomaterials can be used to study pancreatic cancer cell response to a combination of film stiffness and bioactive proteins. We revealed cell-specific responses for PANC1 versus PAN092, stiffness-dependent cellular behaviors, and BMP-dependent cellular responses. Notably, PAN092 did not respond to BMPs while PAN-1 exhibited a strong BMP-dose dependent BMP signaling, which was stronger for bBMP2 than for bBMP4.

Conclusion and Perspectives

Here, using almost full-automated processes, we engineered a bioactive niche with a controlled 3D microenvironment at the micro-scale in which cells can form a microtumor-like tissue. We have also shown that biomimetic film coating can mimic the biophysical conditions of the tumor microenvironment, including stiffness and delivery of adhesion proteins and growth factors like BMP2 and BMP4. We showed that pancreatic cancer cell adhesion, spreading, proliferation and BMP signaling were influenced by both the biomechanical and biochemical signals in a cell-type specific manner. Notably, we observed that cells derived from PAN092 patients did not respond to BMP2 and BMP4, suggesting that these cells may possess Smad mutations reported in previous studies. Interestingly, the biomimetic films may be applied as coating of various polymers, ceramics or composite materials made using different 3D printing systems, thus opening the range of studied biomaterials. In the future, we plan to perform longer-term studied and drug treatment in order to modulate cancer cell signaling and prevent cancer cell growth and metastasis.

Declaration of Competing Interest

None.

Supporting Information

Table S1. µBCA analysis of protein loading on PEM film for EDC30 and EDC70.

Figure S1. Confocal fluorescence images of the PEM film deposited on the Ormocomp 3D scaffold with different mesh sizes.

Figure S2. Confocal fluorescence image of the PEM film coating on the Ormocomp scaffold, where the last PLL layer is marked with FITC (green).

Figure S3. Adhesion, spreading and proliferation of PANC1 cells on control substrates.

Figure S4. Bright field images of PANC1 cells after 120 h of culture on EDC30 loaded with increasing concentrations of either bFN, bBMP2 or bBMP4.

Figure S5. Bright field images of PANC1 cells after 120 h of culture on EDC70, loaded with increasing concentrations of either bFN, bBMP2 or bBMP4.

Figure S6. Adhesion and spreading of PANC1 cells after 16 h of culture on a plastic plate with either sFN, sBMP2 or sBMP4.

Figure S7. Adhesion and spreading of PAN092 cells after 16 h of culture on a plastic plate with either sFN, sBMP2 or sBMP4.

Figure S8. Fluorescence micrographs of PANC1 cells after 16 h of culture on EDC30 with either bFN, bBMP2, or bBMP4.

Figure S9. Fluorescence micrographs of PANC1 cells after 16 h of culture on EDC70 with either bFN, bBMP2, or bBMP4.

Figure S10. Adhesion and spreading of PANC1 cells after 16 h of culture on EDC30 and EDC70 with sFN, sBMP2 and sBMP4.

Figure S11. Adhesion, spreading and proliferation of PAN092 cells on different substrates.

Figure S12. Adhesion and proliferation of PAN092 cells on EDC30 and EDC70 with sFN, sBMP2 and sBMP4.

Figure S13. Fluorescence micrographs of PAN092 cells after 24 h of culture on EDC30 with either bFN, bBMP2 or bBMP4.

Figure S14. Fluorescence micrographs of PAN092 cells after 24 h of culture on EDC70 with either bFN, bBMP2 or bBMP4.

Figure S15. pSmad1/5 signal intensity in (a) PANC1 cells and (b) PAN092 cells cultured on either EDC30 or EDC70 with sFN, sBMP2 and sBMP4.

Acknowledgments

This work was supported by the Fonds Unique Interministériel (FUI) - Banque Publique de l'Innovation (BPI) France, Metropoles of Lyon and Grenoble, Lyonbiopole, Minalogic and La Région Auvergne-Rhône-Alpes (AAP-23 3D ONCOCHIP, N° DOS0062033/0). A. Rengaraj is a postdoctoral fellow funded by Fondation ARC (PDF20171206771). C. Picart is a senior member of the Institut Universitaire de France. Our team is supported by Fondation pour la Recherche Medicale (DEQ20170336746), ERC POC Bioactivecoatings (GA692924) and SATT Bioactivcoatings (160129). We would like to acknowledge the French IMODI cancer consortium for providing us with the patient-derived cancer cells and the financial support to CTIBIOTECH of BPI France and the French Government (PSPC).

References

(1) Bray, F.; Ferlay, J.; Soerjomataram, I.; Siegel, R. L.; Torre, L. A.; Jemal, A. Global Cancer Statistics 2018: GLOBOCAN Estimates of Incidence and Mortality Worldwide for 36 Cancers in 185 Countries. *CA: A Cancer Journal for Clinicians* **2018**, *68* (6), 394–424. https://doi.org/10.3322/caac.21492.

(2) Breslin, S.; O'Driscoll, L. Three-Dimensional Cell Culture: The Missing Link in Drug Discovery. *Drug Discovery Today*. Elsevier Current Trends March 2013, pp 240–249. https://doi.org/10.1016/j.drudis.2012.10.003.

(3) Zhang, Y. J.; Wen, C. L.; Qin, Y. X.; Tang, X. M.; Shi, M. M.; Shen, B. Y.; Fang, Y. Establishment of a Human Primary Pancreatic Cancer Mouse Model to Examine and Investigate Gemcitabine Resistance. *Oncology Reports* **2017**, *38* (6), 3335–3346. https://doi.org/10.3892/or.2017.6026.

(4) Lee, J. W.; Komar, C. A.; Bengsch, F.; Graham, K.; Beatty, G. L. Genetically Engineered Mouse Models of Pancreatic Cancer: The KPC Model (LSL-KrasG12D/+;LSL-Trp53R172H/+;Pdx-1-Cre), Its Variants, and Their Application in Immuno-Oncology Drug Discovery. *Current Protocols in Pharmacology* **2016**, *2016* (June), 14.39.1-14.39.20. https://doi.org/10.1002/cpph.2.

(5) Suklabaidya, S.; Dash, P.; Das, B.; Suresh, V.; Sasmal, P. K.; Senapati, S. Experimental Models of Pancreatic Cancer Desmoplasia. *Lab Invest* **2018**, *98* (1), 27–40. https://doi.org/10.1038/labinvest.2017.127.

(6) Pape, J.; Stamati, K.; Al Hosni, R.; Uchegbu, I. F.; Schatzlein, A. G.; Loizidou, M.; Emberton, M.; Cheema, U. Tissue-Engineering the Fibrous Pancreatic Tumour Stroma Capsule in 3D Tumouroids to Demonstrate Paclitaxel Response. *IJMS* **2021**, *22* (8), 4289. https://doi.org/10.3390/ijms22084289.

(7) Chiellini, F.; Puppi, D.; Piras, A. M.; Morelli, A.; Bartoli, C.; Migone, C. Modelling of Pancreatic Ductal Adenocarcinoma in Vitro with Three-Dimensional Microstructured Hydrogels. *RSC Adv.* **2016**, *6* (59), 54226–54235. https://doi.org/10.1039/C6RA08420F.

(8) Gupta, P.; Pérez-Mancera, P. A.; Kocher, H.; Nisbet, A.; Schettino, G.; Velliou, E. G. A Novel Scaffold-Based Hybrid Multicellular Model for Pancreatic Ductal Adenocarcinoma—Toward a Better Mimicry of the in Vivo Tumor Microenvironment. *Front. Bioeng. Biotechnol.* **2020**, *8*, 290. https://doi.org/10.3389/fbioe.2020.00290.

(9) Totti, S.; Allenby, M. C.; Dos Santos, S. B.; Mantalaris, A.; Velliou, E. G. A 3D Bioinspired Highly Porous Polymeric Scaffolding System for *in Vitro* Simulation of Pancreatic Ductal Adenocarcinoma. *RSC Adv.* **2018**, *8* (37), 20928–20940. https://doi.org/10.1039/C8RA02633E.

(10) Peng, W.; Datta, P.; Ayan, B.; Ozbolat, V.; Sosnoski, D.; Ozbolat, I. T. 3D Bioprinting for Drug Discovery and Development in Pharmaceutics. *Acta Biomaterialia* **2017**, *57*, 26–46. https://doi.org/10.1016/j.actbio.2017.05.025.

(11) Athanasiou, K. A.; Eswaramoorthy, R.; Hadidi, P.; Hu, J. C. Self-Organization and the Self-Assembling Process in Tissue Engineering. *Annual Review of Biomedical Engineering* **2013**, *15* (1), 115–136. https://doi.org/10.1146/annurev-bioeng-071812-152423.

(12) Li, H.; Fan, X.; Houghton, J. M. Tumor Microenvironment: The Role of the Tumor Stroma in Cancer. *Journal of Cellular Biochemistry* **2007**, *101* (4), 805–815. https://doi.org/10.1002/jcb.21159.

(13) Köninger, J.; Giese, T.; Di Mola, F. F.; Wente, M. N.; Esposito, I.; Bachem, M. G.; Giese, N. A.; Büchler, M. W.; Friess, H. Pancreatic Tumor Cells Influence the Composition of the Extracellular Matrix. *Biochemical and Biophysical Research Communications* **2004**, *322* (3), 943–949. https://doi.org/10.1016/j.bbrc.2004.08.008.

(14) Seewaldt, V. ECM Stiffness Paves the Way for Tumor Cells. *Nature Medicine*. 2014. https://doi.org/10.1038/nm.3523.

(15) Migliorini, E.; Valat, A.; Picart, C.; Cavalcanti-Adam, E. A. Tuning Cellular Responses to BMP-2 with Material Surfaces. *Cytokine & Growth Factor Reviews* **2016**, *27*, 43–54. https://doi.org/10.1016/j.cytogfr.2015.11.008.

(16) Jang, I.; Beningo, K. A. Integrins, CAFs and Mechanical Forces in the Progression of Cancer. *Cancers* **2019**, *11* (5). https://doi.org/10.3390/cancers11050721.

(17) Topalovski, M.; Brekken, R. A. Matrix Control of Pancreatic Cancer: New Insights into Fibronectin Signaling. *Cancer Letters* **2016**, *381* (1), 252–258. https://doi.org/10.1016/j.canlet.2015.12.027.
(18) Voorneveld, P. W.; Stache, V.; Jacobs, R. J.; Smolders, E.; Sitters, A. I.; Liesker, A.; S Korkmaz, K.; Lam, S. M.; De Miranda, N. F. C. C.; Morreau, H.; Kodach, L. L.; Hardwick, J. C. H. Reduced Expression of Bone Morphogenetic Protein Receptor IA in Pancreatic Cancer Is Associated with a Poor Prognosis. *British Journal of Cancer* **2013**, *109* (7), 1805–1812. https://doi.org/10.1038/bjc.2013.486.
(19) Daly, A. C.; Randall, R. A.; Hill, C. S. Transforming Growth Factor β-Induced Smad1/5 Phosphorylation in Epithelial Cells Is Mediated by Novel Receptor Complexes and Is Essential for Anchorage-Independent Growth. *MCB* **2008**, *28* (22), 6889–6902. https://doi.org/10.1128/MCB.01192-08.
(20) Gribova, V.; Auzely-Velty, R.; Picart, C. Polyelectrolyte Multilayer Assemblies on Materials Surfaces: From Cell Adhesion to Tissue Engineering. *Chemistry of Materials* **2012**, *24* (5), 854–869. https://doi.org/10.1021/cm2032459.
(21) Detzel, C. J.; Larkin, A. L.; Rajagopalan, P. Polyelectrolyte Multilayers in Tissue Engineering. *Tissue Engineering - Part B: Reviews* **2011**, *17* (2), 101–113. https://doi.org/10.1089/ten.teb.2010.0548.
(22) Richardson, J. J.; Björnmalm, M.; Caruso, F. Technology-Driven Layer-by-Layer Assembly of Nanofilms. *Science*. 2015. https://doi.org/10.1126/science.aaa2491.
(23) Zhang, L.; Zhao, W.; Rudra, J. S.; Haynie, D. T. Context Dependence of the Assembly, Structure, and Stability of Polypeptide Multilayer Nanofilms. *ACS Nano* **2007**. https://doi.org/10.1021/nn700267g.
(24) Tang, Z.; Wang, Y.; Podsiadlo, P.; Kotov, N. A. Biomedical Applications of Layer-by-Layer Assembly: From Biomimetics to Tissue Engineering. *Advanced Materials*. 2006. https://doi.org/10.1002/adma.200600113.
(25) Zelikin, A. N. Drug Releasing Polymer Thin Films: New Era of Surface-Mediated Drug Delivery. *ACS Nano*. 2010. https://doi.org/10.1021/nn100634r.
(26) Ren, K.; Crouzier, T.; Roy, C.; Picart, C. Polyelectrolyte Multilayer Films of Controlled Stiffness Modulate Myoblast Cell Differentiation. *Advanced Functional Materials* **2008**, *18* (9), 1378–1389. https://doi.org/10.1002/adfm.200701297.
(27) Crouzier, T.; Ren, K.; Nicolas, C.; Roy, C.; Picart, C. Layer-By-Layer Films as a Biomimetic Reservoir for RhBMP-2 Delivery : Controlled Differentiation of Myoblasts to Osteoblasts **. **2009**, No. 5, 598–608. https://doi.org/10.1002/smll.200800804.
(28) Schneider, A.; Francius, G.; Obeid, R.; Schwinté, P.; Hemmerlé, J.; Frisch, B.; Schaaf, P.; Voegel, J.-C.; Senger, B.; Picart, C. Polyelectrolyte Multilayers with a Tunable Young's Modulus: Influence of Film Stiffness on Cell Adhesion. *Langmuir* **2006**, *22* (3), 1193–1200. https://doi.org/10.1021/la0521802.
(29) Boudou, T.; Crouzier, T.; Ren, K.; Blin, G.; Picart, C. Multiple Functionalities of Polyelectrolyte Multilayer Films: New Biomedical Applications. *Adv. Mater.* **2010**, *22* (4), 441–467. https://doi.org/10.1002/adma.200901327.
(30) Machillot, P.; Quintal, C.; Dalonneau, F.; Hermant, L.; Monnot, P.; Matthews, K.; Fitzpatrick, V.; Liu, J.; Pignot-Paintrand, I.; Picart, C. Automated Buildup of Biomimetic Films in Cell Culture Microplates for High-Throughput Screening of Cellular Behaviors. *Advanced Materials* **2018**, *30* (27), 1–8. https://doi.org/10.1002/adma.201801097.
(31) Sales, A.; Khodr, V.; Machillot, P.; Chaar, L.; Fourel, L.; Guevara-Garcia, A.; Migliorini, E.; Albigès-Rizo, C.; Picart, C. Differential Bioactivity of Four BMP-Family Members as Function of Biomaterial Stiffness. *Biomaterials* **2022**, *281*, 121363. https://doi.org/10.1016/j.biomaterials.2022.121363.
(32) Rubiano, A.; Delitto, D.; Han, S.; Gerber, M.; Galitz, C.; Trevino, J.; Thomas, R. M.; Hughes, S. J.; Simmons, C. S. Viscoelastic Properties of Human Pancreatic Tumors and in Vitro Constructs to Mimic Mechanical Properties. *Acta Biomaterialia* **2018**, *67*, 331–340. https://doi.org/10.1016/j.actbio.2017.11.037.
(33) Singh, A.; Morris, R. J. The Yin and Yang of Bone Morphogenetic Proteins in Cancer. *Cytokine and Growth Factor Reviews* **2010**, *21* (4), 299–313. https://doi.org/10.1016/j.cytogfr.2010.06.003.

(34) Gribova, V.; Crouzier, T.; Picart, C. A Material's Point of View on Recent Developments of Polymeric Biomaterials: Control of Mechanical and Biochemical Properties. *J. Mater. Chem.* **2011**, *21* (38), 14354. https://doi.org/10.1039/c1jm11372k.
(35) Lee, D.-H.; Bae, C. Y.; Kwon, S.; Park, J.-K. User-Friendly 3D Bioassays with Cell-Containing Hydrogel Modules: Narrowing the Gap between Microfluidic Bioassays and Clinical End-Users' Needs. *Lab Chip* **2015**, *15* (11), 2379–2387. https://doi.org/10.1039/C5LC00239G.
(36) Käpylä, E.; Sorkio, A.; Teymouri, S.; Lahtonen, K.; Vuori, L.; Valden, M.; Skottman, H.; Kellomäki, M.; Juuti-Uusitalo, K. Ormocomp-Modified Glass Increases Collagen Binding and Promotes the Adherence and Maturation of Human Embryonic Stem Cell-Derived Retinal Pigment Epithelial Cells. *Langmuir* **2014**, *30* (48), 14555–14565. https://doi.org/10.1021/la5023642.
(37) Zheng, Y. C.; Zhao, Y. Y.; Zheng, M. L.; Chen, S. L.; Liu, J.; Jin, F.; Dong, X. Z.; Zhao, Z. S.; Duan, X. M. Cucurbit[7]Uril-Carbazole Two-Photon Photoinitiators for the Fabrication of Biocompatible Three-Dimensional Hydrogel Scaffolds by Laser Direct Writing in Aqueous Solutions. *ACS Applied Materials and Interfaces* **2019**. https://doi.org/10.1021/acsami.8b15011.
(38) Wang, H. M.; Chou, Y. T.; Wen, Z. H.; Wang, Z. R.; Chen, C. H.; Ho, M. L. Novel Biodegradable Porous Scaffold Applied to Skin Regeneration. *PLoS ONE* **2013**, *8* (6). https://doi.org/10.1371/journal.pone.0056330.
(39) Kidwell, D. A.; Lee, W.-K.; Perkins, K.; Gilpin, K. M.; O'Shaughnessy, T. J.; Robinson, J. T.; Sheehan, P. E.; Mulvaney, S. P. Chemistries for Making Additive Nanolithography in OrmoComp Permissive for Cell Adhesion and Growth. *ACS Appl. Mater. Interfaces* **2019**, *11* (22), 19793–19798. https://doi.org/10.1021/acsami.9b04096.
(40) Kidwell, D. A.; Lee, W. K.; Perkins, K.; Gilpin, K. M.; O'Shaughnessy, T. J.; Robinson, J. T.; Sheehan, P. E.; Mulvaney, S. P. Chemistries for Making Additive Nanolithography in OrmoComp Permissive for Cell Adhesion and Growth. *ACS Applied Materials and Interfaces* **2019**, *11* (22), 19793–19798. https://doi.org/10.1021/acsami.9b04096.
(41) Lee, J. Y.; An, J.; Chua, C. K. Fundamentals and Applications of 3D Printing for Novel Materials. *Applied Materials Today*. Elsevier Ltd June 2017, pp 120–133. https://doi.org/10.1016/j.apmt.2017.02.004.
(42) Lee, S.; Choi, E.; Cha, M.-J.; Hwang, K.-C. Cell Adhesion and Long-Term Survival of Transplanted Mesenchymal Stem Cells: A Prerequisite for Cell Therapy. *hindawi.com* **2015**. https://doi.org/10.1155/2015/632902.
(43) DuFort, C. C.; Paszek, M. J.; Weaver, V. M. Balancing Forces: Architectural Control of Mechanotransduction. *Nat Rev Mol Cell Biol* **2011**, *12* (5), 308–319. https://doi.org/10.1038/nrm3112.
(44) Guo, W.; Frey, M. T.; Burnham, N. A.; Wang, Y. Substrate Rigidity Regulates the Formation and Maintenance of Tissues. *Biophysical Journal* **2006**, *90* (6), 2213–2220. https://doi.org/10.1529/biophysj.105.070144.
(45) Reuter, S.; Gupta, S. C.; Chaturvedi, M. M.; Aggarwal, B. B. Oxidative Stress, Inflammation, and Cancer: How Are They Linked? *Free radical biology and medicine* **2010**, *49* (11), 1603–1616.
(46) Ehata, S.; Yokoyama, Y.; Takahashi, K.; Miyazono, K. Bi-Directional Roles of Bone Morphogenetic Proteins in Cancer: Another Molecular Jekyll and Hyde?: Bi-Directional Roles of BMPs in Cancer. *Pathol Int* **2013**, *63* (6), 287–296. https://doi.org/10.1111/pin.12067.
(47) Ehata, S.; Yokoyama, Y.; Takahashi, K.; Miyazono, K. Bi-Directional Roles of Bone Morphogenetic Proteins in Cancer: Another Molecular Jekyll and Hyde? *Pathology International* **2013**, *63* (6), 287–296. https://doi.org/10.1111/pin.12067.
(48) Pham, K.; Delitto, D.; Knowlton, A. E.; Hartlage, E. R.; Madhavan, R.; Gonzalo, D. H.; Thomas, R. M.; Behrns, K. E.; George, T. J.; Hughes, S. J.; Wallet, S. M.; Liu, C.; Trevino, J. G. Isolation of Pancreatic Cancer Cells from a Patient-Derived Xenograft Model Allows for Practical Expansion and Preserved Heterogeneity in Culture. *American Journal of Pathology* **2016**, *186* (6), 1537–1546. https://doi.org/10.1016/j.ajpath.2016.02.009.
(49) Akiyama, S. K.; Olden, K.; Yamada, K. M. Fibronectin and Integrins in Invasion and Metastasis. *Cancer and Metastasis Reviews* **1995**, *14* (3), 173–189. https://doi.org/10.1007/BF00690290.

(50) Liu, X. Q.; Fourel, L.; Dalonneau, F.; Sadir, R.; Leal, S.; Lortat-Jacob, H.; Weidenhaupt, M.; Albiges-Rizo, C.; Picart, C. Biomaterial-Enabled Delivery of SDF-1α at the Ventral Side of Breast Cancer Cells Reveals a Crosstalk between Cell Receptors to Promote the Invasive Phenotype. *Biomaterials* **2017**, *127*, 61–74. https://doi.org/10.1016/j.biomaterials.2017.02.035.

(51) Lin, C.; Romero, R.; Sorokina, L. V.; Ballinger, K. R.; Place, L. W.; Kipper, M. J.; Khetani, S. R. A Polyelectrolyte Multilayer Platform for Investigating Growth Factor Delivery Modes in Human Liver Cultures: HEPATOCYTE-GROWTH FACTOR INTERACTIONS ON CHITOSAN-HEPARIN PEMS. *J. Biomed. Mater. Res.* **2018**, *106* (4), 971–984. https://doi.org/10.1002/jbm.a.36293.

(52) Migliorini, E.; Valat, A.; Picart, C.; Cavalcanti-Adam, E. A. *Tuning Cellular Responses to BMP-2 with Material Surfaces*; Elsevier Ltd, 2016; Vol. 27, pp 43–54. https://doi.org/10.1016/j.cytogfr.2015.11.008.

(53) Dalonneau, F.; Liu, X. Q.; Sadir, R.; Almodovar, J.; Mertani, H. C.; Bruckert, F.; Albiges-Rizo, C.; Weidenhaupt, M.; Lortat-Jacob, H.; Picart, C. The Effect of Delivering the Chemokine SDF-1α in a Matrix-Bound Manner on Myogenesis. *Biomaterials* **2014**, *35* (15), 4525–4535. https://doi.org/10.1016/j.biomaterials.2014.02.008.

(54) Koons, G. L.; Mikos, A. G. Progress in Three-Dimensional Printing with Growth Factors. *Journal of Controlled Release* **2019**, *295*, 50–59. https://doi.org/10.1016/j.jconrel.2018.12.035.

(55) Zhou, X.; Hou, Y.; Lin, J. A Review on the Processing Accuracy of Two-Photon Polymerization. *AIP Advances* **2015**. https://doi.org/10.1063/1.4916886.

(56) Ciuciu, A. I.; Cywiński, P. J. Two-Photon Polymerization of Hydrogels-Versatile Solutions to Fabricate Well-Defined 3D Structures. *RSC Advances* **2014**, *4* (85), 45504–45516. https://doi.org/10.1039/c4ra06892k.

(57) Van Landuyt, K. L.; Krifka, S.; Hiller, K. A.; Bolay, C.; Waha, C.; Van Meerbeek, B.; Schmalz, G.; Schweikl, H. Evaluation of Cell Responses toward Adhesives with Different Photoinitiating Systems. *Dental Materials* **2015**, *31* (8), 916–927. https://doi.org/10.1016/j.dental.2015.04.016.

(58) Schizas, C.; Karalekas, D. Mechanical Characteristics of an Ormocomp® Biocompatible Hybrid Photopolymer. *Journal of the Mechanical Behavior of Biomedical Materials* **2011**, *4* (1), 99–106. https://doi.org/10.1016/j.jmbbm.2010.09.010.

(59) Deer, E. L.; González-Hernández, J.; Coursen, J. D.; Shea, J. E.; Ngatia, J.; Scaife, C. L.; Firpo, M. A.; Mulvihill, S. J. Phenotype and Genotype of Pancreatic Cancer Cell Lines. *Pancreas*. Lippincott Williams and Wilkins 2010, pp 425–435. https://doi.org/10.1097/MPA.0b013e3181c15963.

(60) Picollet-D'hahan, N.; Gerbaud, S.; Kermarrec, F.; Alcaraz, J.-P.; Obeid, P.; Bhajun, R.; Guyon, L.; Sulpice, E.; Cinquin, P.; Dolega, M. E.; Wagh, J.; Gidrol, X.; Martin, D. K. The Modulation of Attachment, Growth and Morphology of Cancerous Prostate Cells by Polyelectrolyte Nanofilms. *Biomaterials* **2013**, *34* (38), 10099–10108. https://doi.org/10.1016/j.biomaterials.2013.08.093.

(61) Virtanen, S.; Alarmo, E. L.; Sandström, S.; Ampuja, M.; Kallioniemi, A. Bone Morphogenetic Protein -4 and -5 in Pancreatic Cancer-Novel Bidirectional Players. *Experimental Cell Research* **2011**, *317* (15), 2136–2146. https://doi.org/10.1016/j.yexcr.2011.06.001.

(62) Amrutkar, M.; Aasrum, M.; Verbeke, C. S.; Gladhaug, I. P. Secretion of Fibronectin by Human Pancreatic Stellate Cells Promotes Chemoresistance to Gemcitabine in Pancreatic Cancer Cells. *BMC Cancer* **2019**, *19* (1), 596. https://doi.org/10.1186/s12885-019-5803-1.

(63) Arao, S.; Masumoto, A.; Otsuki, M. B1 Integrins Play an Essential Role in Adhesion and Invasion of Pancreatic Carcinoma Cells. *Pancreas* **2000**, *20* (2), 129–137. https://doi.org/10.1097/00006676-200003000-00004.

(64) Pistritto, G.; Trisciuoglio, D.; Ceci, C.; Alessia Garufi; D'Orazi, G. Apoptosis as Anticancer Mechanism: Function and Dysfunction of Its Modulators and Targeted Therapeutic Strategies. *Aging*. Impact Journals LLC 2016, pp 603–619. https://doi.org/10.18632/aging.100934.

(65) Voorneveld, P. W.; Stache, V.; Jacobs, R. J.; Smolders, E.; Sitters, A. I.; Liesker, A.; S Korkmaz, K.; Lam, S. M.; De Miranda, N. F. C. C.; Morreau, H.; Kodach, L. L.; Hardwick, J. C. H. Reduced Expression of Bone Morphogenetic Protein Receptor IA in Pancreatic Cancer Is Associated with a Poor Prognosis. *British Journal of Cancer* **2013**, *109* (7), 1805–1812. https://doi.org/10.1038/bjc.2013.486.

(66) Gordon, K. J.; Kirkbride, K. C.; How, T.; Blobe, G. C. Bone Morphogenetic Proteins Induce Pancreatic Cancer Cell Invasiveness through a Smad1-Dependent Mechanism That Involves Matrix Metalloproteinase-2. *Carcinogenesis* **2009**, *30* (2), 238–248. https://doi.org/10.1093/carcin/bgn274.
(67) Li, C. S.; Tian, H.; Zou, M.; Zhao, K. W.; Li, Y.; Lao, L.; Brochmann, E. J.; Duarte, M. E. L.; Daubs, M. D.; Zhou, Y. H.; Murray, S. S.; Wang, J. C. Secreted Phosphoprotein 24κD (Spp24) Inhibits Growth of Human Pancreatic Cancer Cells Caused by BMP-2. *Biochemical and Biophysical Research Communications* **2015**, *466* (2), 167–172. https://doi.org/10.1016/j.bbrc.2015.08.124.
(68) Heinecke, K.; Seher, A.; Schmitz, W.; Mueller, T. D.; Sebald, W.; Nickel, J. Receptor Oligomerization and beyond: A Case Study in Bone Morphogenetic Proteins. *BMC Biol* **2009**, *7* (1), 59. https://doi.org/10.1186/1741-7007-7-59.
(69) Singh, P.; Srinivasan, R.; Wig, J. The Smad Family and Its Role in Pancreatic Cancer. *Indian J Cancer* **2011**, *48* (3), 351. https://doi.org/10.4103/0019-509X.84939.
(70) Fitzpatrick, V.; Fourel, L.; Destaing, O.; Gilde, F.; Albigès-Rizo, C.; Picart, C.; Boudou, T. Signal Mingle: Micropatterns of BMP-2 and Fibronectin on Soft Biopolymeric Films Regulate Myoblast Shape and SMAD Signaling. *Sci Rep* **2017**, *7* (1), 41479. https://doi.org/10.1038/srep41479.

For Table of Contents Only